



Effect of chromium substitution on structural, electrical and magnetic properties of NiZn ferrites

Guang-sheng LUO^{1,2}, Yu-hao HONG¹, Wei-ping ZHOU^{1,2},
Zhen-zhi CHENG^{1,2}, Chi-cheng MA¹, Zhong-kai WU¹, Huan-huan HUANG¹

1. School of Materials Science and Engineering, Nanchang University, Nanchang 330031, China;
2. National Laboratory of Solid State Microstructures, School of Physics, Nanjing University, Nanjing 210093, China

Received 15 August 2019; accepted 28 May 2020

Abstract: $\text{Ni}_{0.5}\text{Zn}_{0.5}\text{Fe}_{2-x}\text{Cr}_x\text{O}_4$ ($0 \leq x \leq 0.5$) ferrites were successfully prepared by conventional solid state reaction method to investigate the effect of chromium substitution on the structural, electrical and magnetic properties. X-ray powder diffraction results demonstrate that all the prepared samples are well crystallized single-phase spinel structures without secondary phase. As chromium concentration increases, the lattice parameter and crystallite size gradually decrease. The magnetic measurement indicates that saturation magnetization is substantially suppressed by Cr^{3+} doping, changing from $73.5 \text{ A}\cdot\text{m}^2/\text{kg}$ at $x=0$ to $46.3 \text{ A}\cdot\text{m}^2/\text{kg}$ at $x=0.5$. While the room-temperature electrical resistivity is more than four orders of magnitude enhanced by Cr^{3+} substitution, reaching up to $1.1 \times 10^8 \Omega\cdot\text{cm}$ at $x=0.5$. The dielectric constant monotonously decreases with rising frequency for these ferrites, showing a normal dielectric dispersion behavior. The compositional dependence of dielectric constant is inverse with that of electrical resistivity, which originates from the reduced $\text{Fe}^{2+}/\text{Fe}^{3+}$ electric dipole number by doping, indicating inherent correlation between polarization and conduction mechanism in ferrite.

Key words: NiZn ferrite; chromium doping; electrical resistivity; dielectric properties; saturation magnetization

1 Introduction

Acquiring high performance soft magnetic materials is of demanding needs for the electrified world due to their widespread application in power electronics, electrical machines, microwave devices, transformer core, multilayer inductor, automatics, and computer facilities, etc [1–3]. Spinel ferrite is one of the important soft magnetic materials that are suitable for magnetic and electronic device applications, which have attracted substantial attention for decades [4–8]. In addition to their excellent magnetic characteristics, high electrical resistivity, low eddy current and reduced dielectric

loss in spinel ferrites further widen their application to microwave frequencies [9]. The crystal structure of spinel ferrite is commonly face-centered cubic structure with space group $Fd\bar{3}m$, which is typically expressed in the molecular formula of AB_2O_4 . In this structure, A and B represent four-fold tetrahedral lattice sites (A) and six-fold octahedral lattice sites (B) in the cubic close-packed framework composed by oxygen ions [4]. According to the distribution of cations on the crystallographic site, the spinels can be categorized as normal, inverse and mixed spinel. Among the spinel family, the mixed NiZn ferrites have been intensively scrutinized for their outstanding and versatile properties, including high electrical

Foundation item: Project (11604147) supported by the National Natural Science Foundation of China; Project (M32048) supported by the Foundation of National Laboratory of Solid State Microstructures, China; Project (20142BBE50014) supported by the Jiangxi Province Key Projects of Science and Technology Support Plan, China

Corresponding author: Wei-ping ZHOU; Tel: +86-791-83968964; E-mail: wpzhou@ncu.edu.cn

DOI: 10.1016/S1003-6326(20)65348-1

resistivity, high magnetic susceptibility, low dielectric loss, high quality factor and high chemical stability. Further improving the application frequency and reducing the energy dissipation are key issues for high performance NiZn ferrites. Many efforts have been addressed towards enhancing the electrical resistivity, modification of dielectric and magnetic properties of mixed NiZn ferrites. Substitution is an effective avenue to modify morphological, electrical and magnetic properties, which has been widely adopted by many researchers [9–13]. Chromium ion belongs to 3d traditional metal group with similar radius with ferric ions, and can be readily substituted in the spinel lattice to adjust its physical properties. A few groups have investigated the effect of paramagnetic chromium ions substitution on the magnetic and electrical properties of NiZn ferrites. For example, KUMAIR et al [14] reported that the dielectric constant, dielectric loss and AC conductivity decrease with increasing Cr^{3+} substitution in ZnFe_2O_4 . BIRAJDAR et al [15] found that the saturation magnetization for $\text{Ni}_{0.7}\text{Zn}_{0.3}\text{Fe}_2\text{O}_4$ is suppressed by chromium doping. GABAL et al [16] observed that the Curie temperature of $\text{Ni}_{0.8}\text{Zn}_{0.2}\text{Fe}_2\text{O}_4$ decreases by Cr substitution. Above all, $\text{Ni}_{0.5}\text{Zn}_{0.5}\text{Fe}_2\text{O}_4$ exhibits the largest saturation magnetization in the NiZn ferrite series [17,18], whereas the effect of Cr^{3+} ion substitution on its properties has not been systematically reported in the literature. Therefore, it is highly needed to further investigate the Cr substituted NiZn ferrite to clarify substitution mechanism and furnish assorted properties.

In this work, we have comprehensively investigated the role of chromium substitution on the structural, morphological, electrical and magnetic properties of $\text{Ni}_{0.5}\text{Zn}_{0.5}\text{Fe}_2\text{O}_4$ ferrite. It is found that the electrical resistivity is effectively enhanced as much as more than four orders of magnitude by chromium doping. The underlying mechanism of chromium substitution effect on the physical properties of NiZn ferrite is substantially discussed.

2 Experimental

$\text{Ni}_{0.5}\text{Zn}_{0.5}\text{Fe}_{2-x}\text{Cr}_x\text{O}_4$ ($x=0, 0.1, 0.2, 0.3, 0.4$ and 0.5) polycrystalline samples were synthesized by

traditional ceramics method. High purity raw materials of NiO (99%), ZnO (99%), Fe_2O_3 (99%) and Cr_2O_3 (99%) were weighed according to the stoichiometric ratio. Firstly, these raw powders were completely mixed and milled in alcohol by agate balls for 4 h in a planetary ball mill, and then dried and calcined at 1100 °C for 3 h. A second ball-milling was performed following an intermediate manual grinding in an agate mortar for these pre-sintered powders. Subsequently, these powders were pressed into pellets under uniaxial dry pressing at 15 MPa for 5 min, and then sintered at 1400 °C for 4 h with a heating rate of 5 °C/min. The as-prepared pellets were polished into plates with a thickness of 0.8 mm and coated with silver electrode on both surfaces.

The phase purity was characterized by X-ray powder diffraction (BRUKER, D8 Focus) equipped with Cu $K_{\alpha 1}$ radiation ($\lambda=1.54056 \text{ \AA}$) at room temperature. The morphology and element mapping were carried out by scanning electron microscope (SEM) and energy dispersive spectrometer (EDS) (Hitachi, S-3400N II). The dielectric constant and tangent loss were measured by a precise impedance analyzer (Agilent 4284A LCR meter) at room temperature. The current–voltage curves were measured by two-probe method at room temperature. The magnetic properties were measured by vibrating sample magnetometer (VSM, Lakeshore-7300) at room temperature.

3 Results and discussion

3.1 X-ray diffraction

Figure 1(a) shows the XRD patterns of $\text{Ni}_{0.5}\text{Zn}_{0.5}\text{Fe}_{2-x}\text{Cr}_x\text{O}_4$ ceramics collected at room temperature. All of the Bragg peaks can be well indexed in a cubic spinel structure with space group of $Fd3m$ without secondary phase, indicating that Cr^{3+} ions were incorporated into the spinel lattice. To clearly demonstrate the effect of Cr^{3+} substitution on the structure, magnified XRD patterns of the strongest (311) peak are shown in Fig. 1(b). Obviously, the peak position gradually shifts to higher angle with increasing Cr^{3+} concentration, indicating that the spinel structure gradually shrinks with substitution. To quantitatively analyze the structural evolution by substitution, the lattice parameters are calculated from the XRD patterns by the following equation:

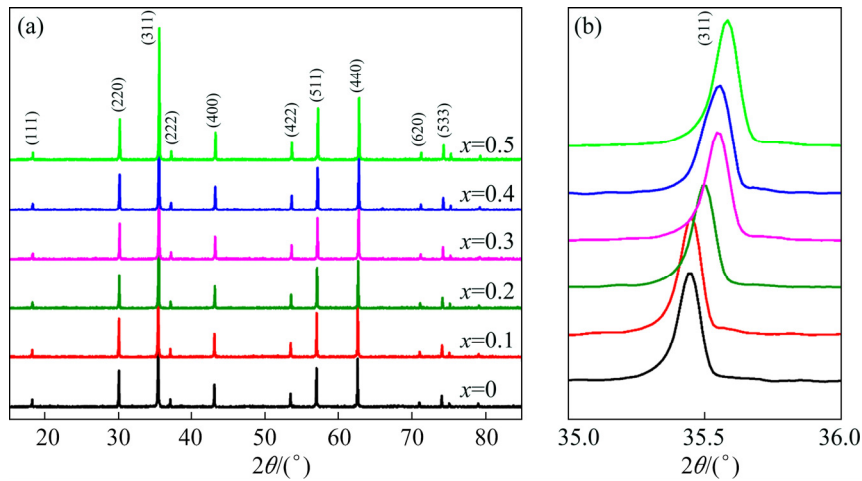


Fig. 1 XRD patterns of $\text{Ni}_{0.5}\text{Zn}_{0.5}\text{Fe}_{2-x}\text{Cr}_x\text{O}_4$ ferrites measured at room temperature (a) and magnified (311) peak of these XRD patterns (b)

$$a = \frac{\lambda \sqrt{(h^2 + k^2 + l^2)}}{2 \sin \theta} \quad (1)$$

where $(h k l)$ are diffraction indices, θ represents the diffraction angle of the $(h k l)$ peak, and λ is the wavelength of X-ray.

As shown in Fig. 2, the lattice parameters of $\text{Ni}_{0.5}\text{Zn}_{0.5}\text{Fe}_{2-x}\text{Cr}_x\text{O}_4$ ferrites monotonously decrease from 8.390 Å for parent compound to 8.361 Å for $x=0.5$ with increasing Cr^{3+} concentration. This behavior has a direct relationship with the size of the substituted ions. As reported previously, the ionic radius of Cr^{3+} (0.615 Å) is smaller compared with that of Fe^{3+} (0.645 Å) [19]. According to the Vegard's law, when a portion of Fe^{3+} ions are substituted by Cr^{3+} ions, the size of the unit cell shrinks, leading to decreased lattice constant. Similar phenomenon was also observed in other

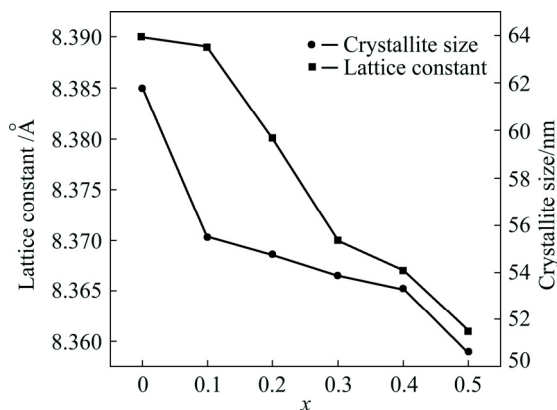


Fig. 2 Lattice constant and crystallite size of NiZn ferrites as function of chromium substitution concentration

Cr-substituted ferrites [20]. The average crystallite size is calculated using the Scherrer's equation: $D=0.89\lambda/\beta\cos\theta$, where λ is the wavelength of X-ray, β is the full width at the half-maximum in radians, and θ is the angle of the most intense (311) diffraction peak. The crystallite size substantially decreases from 62 to 51 nm with increasing Cr^{3+} concentration, as shown in Fig. 2.

3.2 SEM

Microstructure and morphology of the ferrites could provide valuable information for understanding the doping effect on the physical and chemical properties of ferrite. The cross-section SEM measurements were conducted to investigate the effect of chromium doping on the particle size and morphology of NiZn ferrite, as shown in Fig. 3. All the samples are densely sintered and the Cr^{3+} doping has an impact on the structural morphology and particle size of NiZn ferrites. More specifically, rounded grains with the average size of 3.9 μm are prevalent for undoped samples. While the average particle size decreases to 2.9 μm at $x=0.1$. However, the grains grow rapidly and merge together by reducing grain boundaries at $x=0.2$ and 0.3. Further increasing the doping concentration leads to discrete grains with rounded shape, as shown at $x=0.4$ and 0.5. The average grain size increases from 2.1 μm at $x=0.4$ to 4.5 μm at $x=0.5$. In Fig. 4, the element mapping of sample measured by EDS at $x=0.4$ shows that the elements of Ni, Zn, Fe, Cr, O are all evenly distributed in the sample without obvious element aggregation.

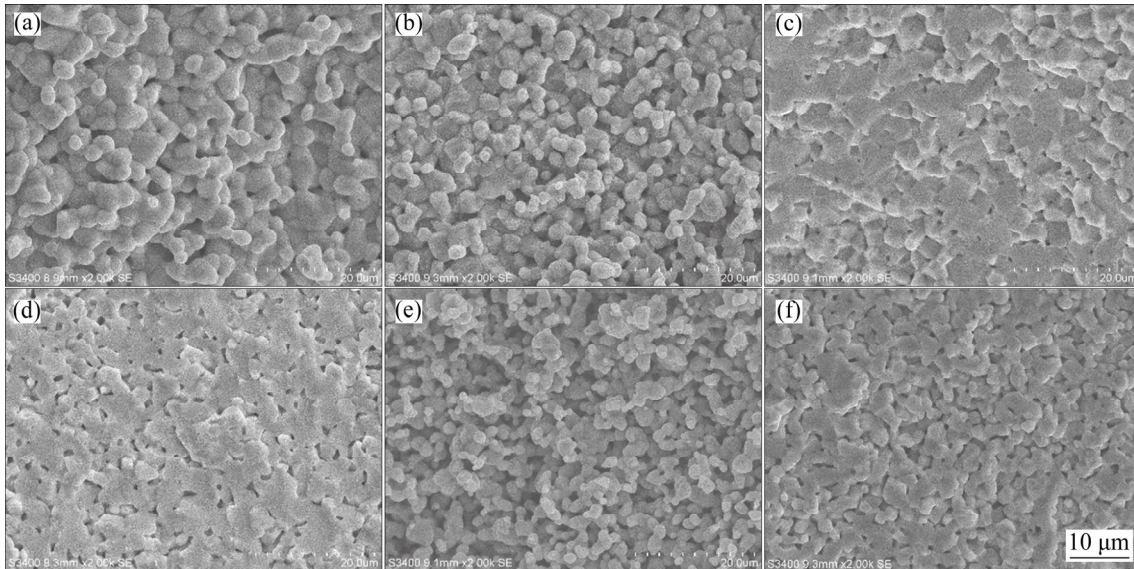


Fig. 3 SEM images of $\text{Ni}_{0.5}\text{Zn}_{0.5}\text{Fe}_{2-x}\text{Cr}_x\text{O}_4$ ferrites: (a) $x=0$; (b) $x=0.1$; (c) $x=0.2$; (d) $x=0.3$; (e) $x=0.4$; (f) $x=0.5$

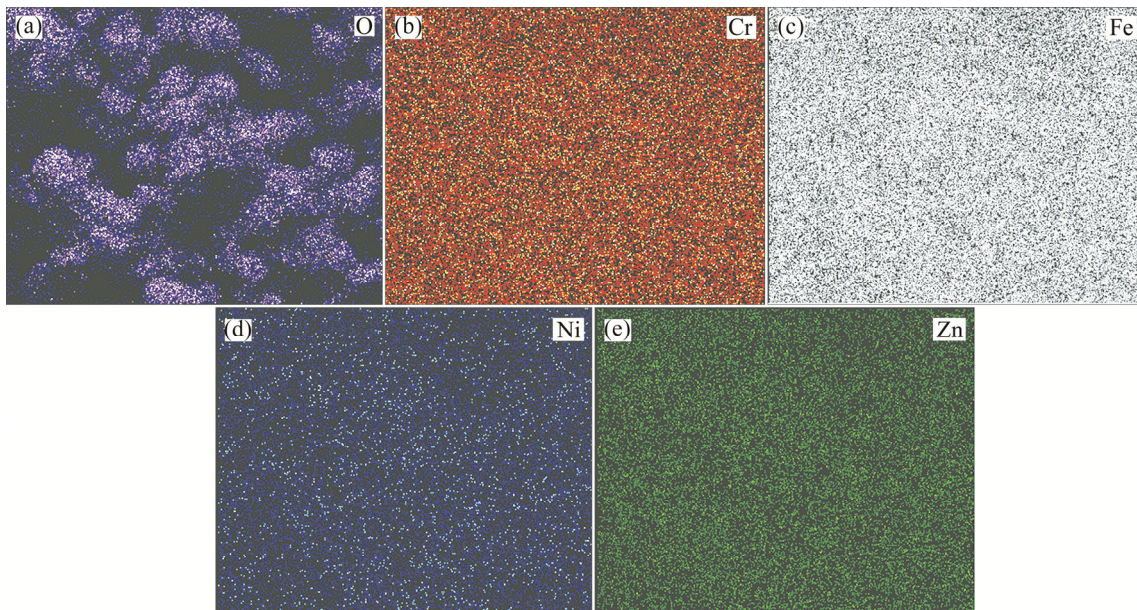


Fig. 4 Element mapping of $\text{Ni}_{0.5}\text{Zn}_{0.5}\text{Fe}_{1.6}\text{Cr}_{0.4}\text{O}_4$ sample: (a) O; (b) Cr; (c) Fe; (d) Ni; (e) Zn

3.3 Magnetic properties

The magnetic hysteresis loops of $\text{Ni}_{0.5}\text{Zn}_{0.5}\text{Fe}_{2-x}\text{Cr}_x\text{O}_4$ ferrites measured at room temperature are shown in Fig. 5. All the samples exhibit typical S-shaped magnetic loops with a tiny coercive field. It can be clearly noted that the shape of $M-H$ loops varies with Cr^{3+} substitution, which is the most obvious in the saturated region. The saturation magnetization, coercive field and remanence of $\text{Ni}_{0.5}\text{Zn}_{0.5}\text{Fe}_{2-x}\text{Cr}_x\text{O}_4$ ferrites are extracted from $M-H$ loops, which are presented in Table 1. The saturation magnetization is plotted as a function of Cr^{3+} -doping level, as shown in the inset

of Fig. 5. For the undoped compound ($x=0$), the saturation magnetization is $73.5 \text{ A}\cdot\text{m}^2/\text{kg}$, which is akin with the results ($70.13\text{--}84 \text{ A}\cdot\text{m}^2/\text{kg}$) reported by our group [21, 22] and other groups [23,24]. It can be seen that the saturation magnetization is approximately linearly suppressed by Cr^{3+} doping and reaches up to $46.3 \text{ A}\cdot\text{m}^2/\text{kg}$ at $x=0.5$. The effect of Cr^{3+} substitution on the magnetic properties of NiZn ferrites can be explained by the collinear ferrimagnetic structure of spinel. As mentioned earlier, there are two different lattice sites, i.e. four-fold tetrahedral lattice sites (A) and six-fold octahedral lattice sites (B), which can be occupied

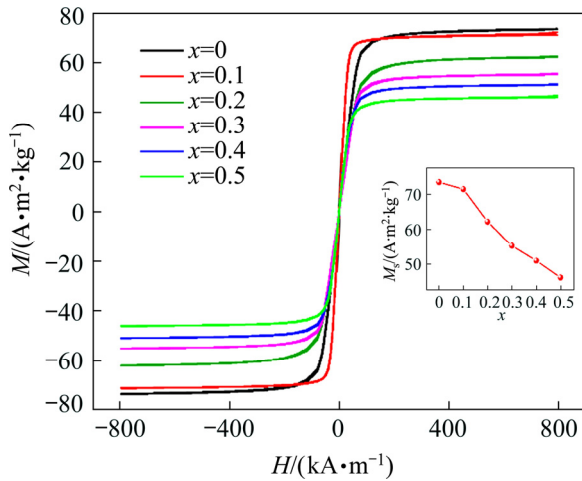


Fig. 5 Magnetic hysteresis loops of $\text{Ni}_{0.5}\text{Zn}_{0.5}\text{Fe}_{2-x}\text{Cr}_x\text{O}_4$ ferrites measured at room temperature (The inset shows the saturation magnetization (M_s) of NiZn ferrites as a function of Cr substitution level)

by cations in spinel structure. Each ion at the A site has 12 B-site ions as the nearest neighbors. The strength of magnetic exchange interactions between magnetic atoms on A sites and B sites are dominant over than that of A–A and B–B interactions within each sublattice. Antiparallel arrangement between A- and B-site spins is formed due to the large negative A–B interaction originating from superexchange interaction among magnetic ions via oxygen [5]. Therefore, the net magnetization of spinel ferrite can be expressed as the subtraction between the magnetization of B site sublattice (M_B) and the that of A site sublattice (M_A), i.e. $M=M_B-M_A$. The occupation preference of metal ions in spinel ferrite has an impact on its magnetic properties. Zn^{2+} ions have a strong tendency to occupy the A site [25], while Ni^{2+} and Cr^{3+} ions are more likely to occupy octahedral B site because of favorable crystal-field effects [19], whereas Fe^{3+} ions can distribute both on A and B sites. Therefore, the doped- Cr^{3+} ions would occupy the B site by replacement of Fe^{3+} ions. The magnetic moment of Cr^{3+} (3 Bohr magnetos) is smaller than that of Fe^{3+} (5 Bohr magnetos). The substitution of high magnetic moment Fe^{3+} ions by low magnetic moment Cr^{3+} ions on octahedral site could lead to a decrease of the magnetic moment of B sublattice. As a result, the net magnetic moment of NiZn ferrite ($M=M_B-M_A$) decreases with the addition chromium concentration. Interestingly, as shown in Table 1, the coercive field and remanence show

trivial variation with chromium substitution and all exhibit miniscule values, indicating the excellent soft magnetic characteristic of these ferrites.

Table 1 Saturation magnetization, coercive field and remanence of $\text{Ni}_{0.5}\text{Zn}_{0.5}\text{Fe}_{2-x}\text{Cr}_x\text{O}_4$ ferrites

x	Saturation magnetization/ ($\text{A}\cdot\text{m}^2\cdot\text{kg}^{-1}$)	Coercive field/ ($\text{A}\cdot\text{m}^{-1}$)	Remanence/ ($\text{A}\cdot\text{m}^2\cdot\text{kg}^{-1}$)
0	73.5	159.2	0.155
0.1	71.5	87.5	0.19
0.2	62.3	143.2	0.115
0.3	55.3	175.1	0.132
0.4	51.1	167.1	0.195
0.5	46.3	175.1	0.165

3.4 Resistivity

The electrical properties of ferrites are very important for their applications at high frequency. In order to investigate the role of chromium doping on electrical properties of NiZn ferrite, the current density as a function of applied field (J – V) of these samples were measured by the two-probe method at room temperature, as presented in Fig. 6(a). The almost linear dependence of current density on applied field in the double logarithmic curve implies the ohmic behavior of these samples. The electrical resistivity (ρ) is calculated by

$$\rho = \frac{RS}{L} \quad (2)$$

where R is the measured resistance, S is the cross-sectional area of the samples, and L is the sample thickness.

As demonstrated in Fig. 6(b), it is observed that electrical resistivity is substantially enhanced by doping chromium ions in NiZn ferrite, from $5.3 \times 10^3 \Omega\cdot\text{cm}$ at $x=0$ to $1.1 \times 10^8 \Omega\cdot\text{cm}$ at $x=0.5$, corresponding to an enhancement of more than four orders of magnitude. The high electrical resistivity of Cr^{3+} -doped NiZn ferrite is favorable for high frequency applications. The variation of resistivity can be understood by the combination effect of Cr^{3+} substitution and grain size. The electric transport mechanism in ferrites has been interpreted by the electron hopping between ions of the same element with different valence states on octahedral sites [26], such as the most common case of $\text{Fe}^{2+}/\text{Fe}^{3+}$ randomly located on octahedral sites. The Cr^{3+} ion

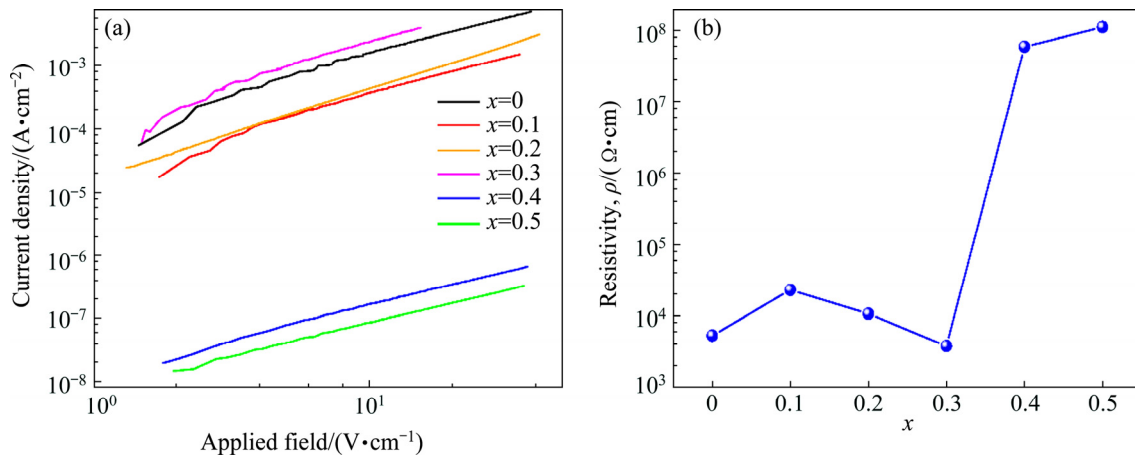


Fig. 6 J - V curves of $\text{Ni}_{0.5}\text{Zn}_{0.5}\text{Fe}_{2-x}\text{Cr}_x\text{O}_4$ measured at room temperature (a) and electrical resistivity of $\text{Ni}_{0.5}\text{Zn}_{0.5}\text{Fe}_{2-x}\text{Cr}_x\text{O}_4$ deduced from J - V curves (b)

has a strong preference towards occupying the octahedral sites. The replacement of Fe^{3+} by Cr^{3+} in NiZn ferrite reduces the number of Fe^{3+} on octahedral site. Since the chromium ions do not contribute to the conduction process due to its stable valence state [27], the number of electrons hopping between Fe^{2+} and Fe^{3+} decreases, leading to an enhanced resistivity. However, abnormal decrease of electrical resistivity at $x=0.2$ and 0.3 is observed. The electrical properties of ferrites are also strongly dependent on the grain boundaries, defects, porosity and stoichiometry. It is known that the inhomogeneous dielectric structure of ferrite ceramic is composed of conductive grains and insulating grain boundaries [28,29]. Previous reports indicated that an increase in density of grain boundaries in a ferrite system increases the electrical resistivity of the system [19,27]. From Fig. 3, it is observed that the grains grow rapidly and merge together for $x=0.2$ and 0.3 samples. Larger grain size indicates less number of insulating boundaries, which is beneficial to the current flow across the sample. Moreover, the larger grain size means larger surface contact area which promotes the electron flow. Other factors such as porosity and stoichiometry may also contribute to the electric properties, since the unusual grain growth reduces the porosity of the samples. Therefore, the major reason for the decrease in electrical resistivity for $x=0.2$ and 0.3 samples is ascribed to the decline of grain boundary density due to grain growth. In contrary, $x=0.4$ and 0.5 samples show a smaller grain size with pore structure, which contains greater number of insulating grain boundaries that

hinder the transport of electrons, leading to the high resistivity.

3.5 Dielectric properties

NiZn ferrite is an important kind of dielectric materials [30]. The variation of dielectric constant (ϵ) for Cr-doped NiZn ferrites as a function of measured frequency in the range from 100 Hz to 1 MHz at room temperature is presented in Fig. 7(a). For the low doping samples, a colossal dielectric constant in the order of 10^3 – 10^5 appears at low frequencies, which may be attributed to the interfacial polarization correlated with the inhomogeneity of the conductivity between grains and grain boundaries [31]. Similar phenomenon was observed in Ho- and Sm-doped Ni ferrites [32]. The dielectric constant continuously decreases with rising measured frequency, showing a normal dielectric dispersion behavior. It is reported that the dielectric relaxation and conductivity in ferrites have similar activation energies, implying an inherent correlation between these two processes in ferrites [33]. The dielectric polarization process can be understood by the electron hopping conduction between ferrous and ferric ions. Electric dipoles are induced due to the electron hopping between Fe^{2+} and Fe^{3+} ions when alternating electric field is applied, resulting in an electric polarization in the ferrites. However, the hopping process of charge carriers gradually gets out of sync with the frequency of applied alternating electric field, rendering the reduction of dielectric constant. According to the Koops theory [28], the dispersion behavior of dielectric constant was ascribed to the

relaxation of interfacial polarization at grain boundaries, in which conductive grains contribute to the high-frequency response and grain boundaries dominate the colossal low-frequency response. The compositional dependence of dielectric permittivity measured at 10 kHz is presented in Fig. 7(b). A strong relevance between dielectric constant and electrical resistivity behavior of ferrite can be observed by comparison with Fig. 6(b). It is found that the high electrical resistivity sample manifests the lower dielectric constant, further supporting the inherent correlation between the polarization process and conduction process in ferrites. The dielectric constant is suppressed with increasing Cr concentration, originating from the reduced $\text{Fe}^{2+}/\text{Fe}^{3+}$ electric dipole number by doping. The abnormal increase of dielectric constant for $x=0.3$ sample is consistent with its low resistivity, which strongly correlates with its large grain size with less insulating grain boundaries.

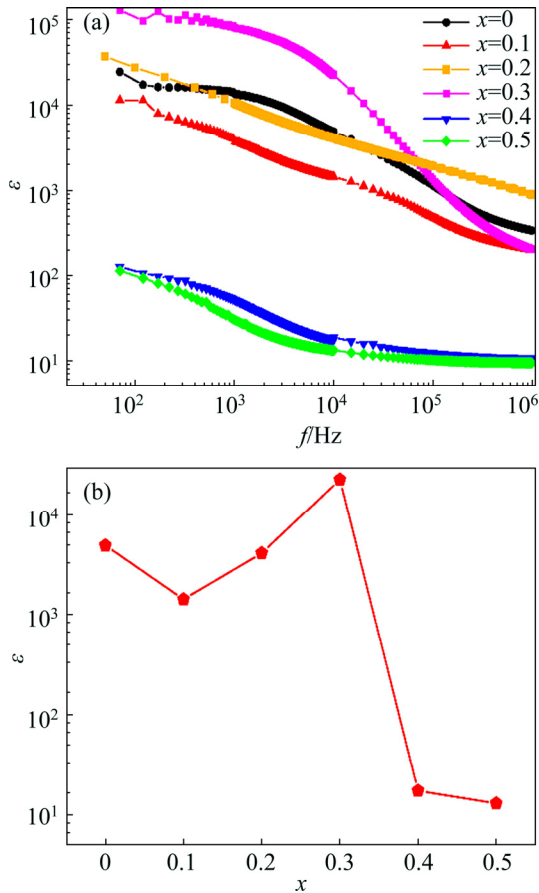


Fig. 7 Frequency dependence of dielectric constant for $\text{Ni}_{0.5}\text{Zn}_{0.5}\text{Fe}_{2-x}\text{Cr}_x\text{O}_4$ ferrites (a) and compositional dependence of dielectric constant for $\text{Ni}_{0.5}\text{Zn}_{0.5}\text{Fe}_{2-x}\text{Cr}_x\text{O}_4$ ferrites measured at 10 kHz (b)

The dielectric tangent loss ($\tan \delta$) is an important parameter reflecting the energy dissipation during polarization process, as demonstrated in Fig. 8(a). It is observed that the tangent loss systematically reduces with increasing measured frequency. A tangent loss peak is observed for $x=0.3$ sample at the frequency about 300 kHz, which can be attributed to the hopping frequency of electron between Fe^{2+} and Fe^{3+} equals to the frequency of the applied field [21]. For $x=0.4$ and 0.5 samples, the tangent loss value is largely suppressed compared with those low doping samples, especially at high frequencies, implying its potential application in high frequency devices. The tangent loss as a function of chromium concentration is presented in Fig. 8(b), which decreases with increasing chromium doping.

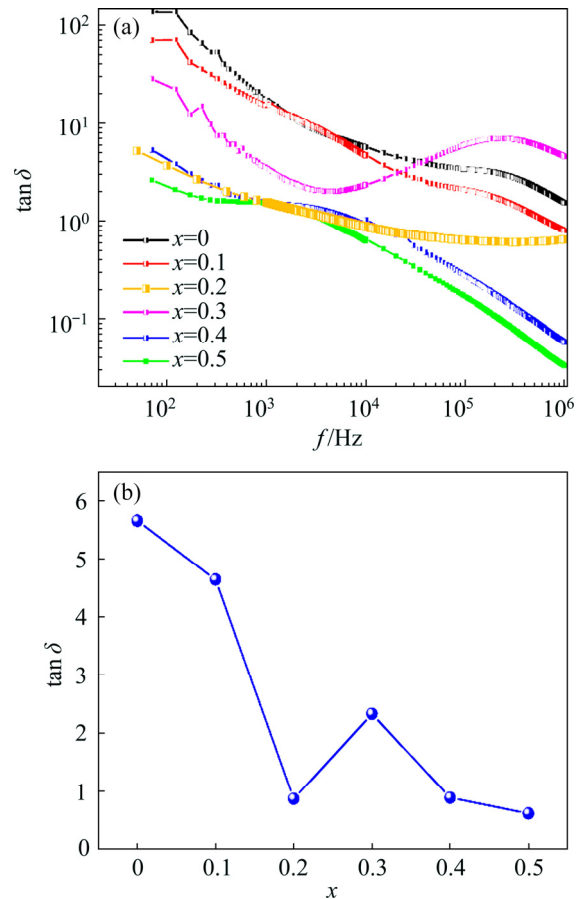


Fig. 8 Frequency dependence of dielectric tangent loss for $\text{Ni}_{0.5}\text{Zn}_{0.5}\text{Fe}_{2-x}\text{Cr}_x\text{O}_4$ ferrites (a) and compositional dependence of dielectric tangent loss for $\text{Ni}_{0.5}\text{Zn}_{0.5}\text{Fe}_{2-x}\text{Cr}_x\text{O}_4$ ferrites measured at 10 kHz (b)

4 Conclusions

- (1) The polycrystalline $\text{Ni}_{0.5}\text{Zn}_{0.5}\text{Fe}_{2-x}\text{Cr}_x\text{O}_4$

($0 \leq x \leq 0.5$) ferrites were prepared by solid state reaction method. Well crystallized single-phase spinel structure without impurity phase for all the prepared samples were confirmed by X-ray powder diffraction technique. The crystal parameter and crystallite size decrease monotonously with the addition of chromium content.

(2) SEM results show the compact and dense microscopic morphology structure of these ferrites. EDS mapping indicates that all elements are evenly distributed in the sample without obvious element aggregation.

(3) Soft ferromagnetic hysteresis loops with tiny coercive field are observed for all the compositions at room temperature. Chromium substitution leads to substantial suppression of the saturation magnetization.

(4) Normal dielectric dispersion behavior is observed for all the compositions in which the permittivity decreases with increasing frequency. The compositional dependence of electrical resistivity is enhanced with chromium substitution, while the dielectric constant shows the opposite tendency.

References

- [1] SILVEYRA J M, FERRARA E, HUBER D L, MONSON T C. Soft magnetic materials for a sustainable and electrified world [J]. *Science*, 2018, 362(6413): 418–428.
- [2] FIORILLO F, FERRARA E, COÏSSON M, BEATRICE C, BANU N. Magnetic properties of soft ferrites and amorphous ribbons up to radiofrequencies [J]. *Journal of Magnetism and Magnetic Materials*, 2010, 322(9–12): 1497–1504.
- [3] SUNDAY K J, TAHERI M L. NiZnCu-ferrite coated iron powder for soft magnetic composite applications [J]. *Journal of Magnetism and Magnetic Materials*, 2018, 463: 1–6.
- [4] HARRIS V G. Modern microwave ferrites [J]. *IEEE Transactions on Magnetics*, 2012, 48(3): 1075–1104.
- [5] ÖZGÜR Ü, ALIVOV Y, MORKOÇ H. Microwave ferrites, part 1: Fundamental properties [J]. *Journal of Materials Science: Materials in Electronics*, 2009, 20(9): 789–834.
- [6] GE Yi-cheng, WANG Zhi-long, YI Mao-zhong, RAN Li-ping. Fabrication and magnetic transformation from paramagnetic to ferrimagnetic of ZnFe₂O₄ hollow spheres [J]. *Transactions of Nonferrous Metals Society of China*, 2019, 29: 1503–1509.
- [7] SARTAJ AZIZ H, ALI KHAN R, SHAH F, ISMAIL B, NISAR J, MUJTABA SHAH S, RAHIM A, RAHMAN KHAN A. Improved electrical, dielectric and magnetic properties of Al–Sm co-doped NiFe₂O₄ spinel ferrites nanoparticles [J]. *Materials Science and Engineering B*, 2019, 243: 47–53.
- [8] REDDY D H K, YUN Y S. Spinel ferrite magnetic adsorbents: Alternative future materials for water purification? [J]. *Coordination Chemistry Reviews*, 2016, 315: 90–111.
- [9] JACOBO S E, BERCOFF P G. Structural and electromagnetic properties of yttrium-substituted Ni–Zn ferrites [J]. *Ceramics International*, 2016, 42(6): 7664–7668.
- [10] LUO Guang-sheng, ZHOU Wei-ping, LI Jian-de, JIANG Gui-wen, TANG Shao-long, DU You-wei. Effect of Cu ion substitution on structural and dielectric properties of Ni–Zn ferrites [J]. *Transactions of Nonferrous Metals Society of China*, 2015, 25(11): 3678–3684.
- [11] WANG Sea-Fue, HSU Yung-Fu, CHOU Kai-Mou, TSAI Jeng-Ting. Effects of co-dopants on the magnetic properties of Ni–Zn ferrites [J]. *Journal of Magnetism and Magnetic Materials*, 2015, 374: 402–410.
- [12] IKRAM S, JACOB J, ARSHAD M I, MAHMOOD K, ALI A, SABIR N, AMIN N, HUSSAIN S. Tailoring the structural, magnetic and dielectric properties of Ni–Zn–CdFe₂O₄ spinel ferrites by the substitution of lanthanum ions [J]. *Ceramics International*, 2019, 45(3): 3563–3569.
- [13] JUNAID M, KHAN M A, AKHTAR M N, HUSSAIN A, WARSIM F. Impact of indium substitution on dielectric and magnetic properties of Cu_{0.5}Ni_{0.5}Fe_{2-x}O₄ ferrite materials [J]. *Ceramics International*, 2019, 45(10): 13431–13437.
- [14] KUMARI N, KUMAR V, SINGH S K. Effect of Cr³⁺ substitution on properties of nano-ZnFe₂O₄ [J]. *Journal of Alloys and Compounds*, 2015, 622: 628–634.
- [15] BIRAJDAR A A, SHIRSATH S E, KADAM R H, PATANGE S M, LOHAR K S, MANE D R, SHITRE A R. Role of Cr³⁺ ions on the microstructure development, and magnetic phase evolution of Ni_{0.7}Zn_{0.3}Fe₂O₄ ferrite nanoparticles [J]. *Journal of Alloys and Compounds*, 2012, 512(1): 316–322.
- [16] GABAL M A, AL ANGARI Y M, AL-AGEL F A. Cr-substituted Ni–Zn ferrites via oxalate decomposition: Structural, electrical and magnetic properties [J]. *Journal of Magnetism and Magnetic Materials*, 2015, 391: 108–115.
- [17] AL-GHAMDI A A, AL-HAZMI F S, MEMESH L S, SHOKR F S, BRONSTEIN L M. Effect of mechanochemical synthesis on the structure, magnetic and optical behavior of Ni_{1-x}Zn_xFe₂O₄ spinel ferrites [J]. *Ceramics International*, 2017, 43(8): 6192–6200.
- [18] KAMBALE R C, ADHATE N R, CHOUGULE B K, KOLEKAR Y D. Magnetic and dielectric properties of mixed spinel Ni–Zn ferrites synthesized by citrate–nitrate combustion method [J]. *Journal of Alloys and Compounds*, 2010, 491(1–2): 372–377.
- [19] PANDA R K, MUDULI R, JAYARAO G, SANYAL D, BEHERA D. Effect of Cr³⁺ substitution on electric and magnetic properties of cobalt ferrite nanoparticles [J]. *Journal of Alloys and Compounds*, 2016, 669: 19–28.
- [20] AZAM M, ADEELA N, KHAN U, RIAZ S, IQBAL M, NASEEM S. Structural and magnetic investigations of Cr substituted NiFe₂O₄ nanostructures [J]. *Journal of Alloys and Compounds*, 2017, 698: 228–233.
- [21] LUO G S, ZHOU W P, LI J D, JIANG G W, TANG S L, DU Y W. Investigation on nickel concentration dependence structural, dielectric and magnetic properties of Ni–Zn

- ferrites [J]. Journal of Materials Science: Materials in Electronics, 2018, 29: 12489–12495.
- [22] LUO G S, ZHOU W P, LI J D, ZHOU Z Y, JIANG G W, LI W S, TANG S L, DU Y W. The influence of Nd^{3+} ions doping on structural, dielectric and magnetic properties of Ni–Zn ferrites [J]. Journal of Materials Science: Materials in Electronics, 2017, 28: 7259–7263
- [23] KÖSEOĞLU Y. Structural and magnetic properties of Cr doped NiZn-ferrite nanoparticles prepared by surfactant assisted hydrothermal technique [J]. Ceramics International, 2015, 41(5): 6417–6423.
- [24] WU Xue-hang, WU Wen-wei, QIN Li-qin, WANG Kai-tuo, OU Shi-qian, ZHOU Kai-wen, FAN Yan-jin. Structure and magnetic properties evolution of nickel-zinc ferrite with lanthanum substitution [J]. Journal of Magnetism and Magnetic Materials, 2015, 379: 232–238.
- [25] SHINDE T J, GADKARI A B, VASAMBEKAR P N. Magnetic properties and cation distribution study of nanocrystalline Ni–Zn ferrites [J]. Journal of Magnetism and Magnetic Materials, 2013, 333: 152–155.
- [26] JONKER G H. Analysis of the semiconducting properties of cobalt ferrite [J]. Journal of Physics and Chemistry of Solids, 1959, 9(2): 165–175.
- [27] PATANGE S M, SHIRSATH S E, TOKSHA B G, JADHAV S S, JADHAV K M. Electrical and magnetic properties of Cr^{3+} substituted nanocrystalline nickel ferrite [J]. Journal of Applied Physics, 2009, 106(2): 23914.1–23914.7.
- [28] KOOPS C G. On the dispersion of resistivity and dielectric constant of some semiconductors at audiofrequencies [J]. Physical Review, 1951, 83(1): 121–124.
- [29] DEVAN R S, KOLEKAR Y D, CHOUGULE B K. Effect of cobalt substitution on the properties of nickel–copper ferrite [J]. Journal of Physics: Condensed Matter, 2006, 18(43): 9809–9821.
- [30] WANG Yan-bin, JIE Wen-jing, YANG Chao, WEI Xian-hua, HAO Jian-hua. Colossal permittivity materials as superior dielectrics for diverse applications [J]. Advanced Functional Materials, 2019: 1808118.1–1808118.27.
- [31] BOBNAR V, PRONIN A V, RITUS A I, VOLKOV A A, LOIDL A, LUNKENHEIMER P. Origin of apparent colossal dielectric constants [J]. Physical Review B, 2002, 66(5): 52105.1–52105.4.
- [32] BHARATHI K K, MARKANDEYULU G, RAMANA C V. Structural, magnetic, electrical, and magnetoelectric properties of Sm-and Ho-substituted nickel ferrites [J]. The Journal of Physical Chemistry C, 2010, 115(2): 554–560.
- [33] ZHENG Hui, WENG Wen-jian, HAN Gao-rong, DU Pi-yi. Colossal permittivity and variable-range-hopping conduction of polarons in $\text{Ni}_{0.5}\text{Zn}_{0.5}\text{Fe}_2\text{O}_4$ ceramic [J]. The Journal of Physical Chemistry C, 2013, 117(25): 12966–12972.

Cr 离子掺杂对 NiZn 铁氧体结构、 电学及磁学性能的影响

罗广圣^{1,2}, 洪宇昊¹, 周卫平^{1,2}, 程振之^{1,2}, 马驰骋¹, 吴仲楷¹, 黄欢欢¹

1. 南昌大学 材料科学与工程学院, 南昌 330031;

2. 南京大学 物理学院 固体微结构国家重点实验室, 南京 210093

摘要: 通过常规的固相烧结法成功制备 $\text{Ni}_{0.5}\text{Zn}_{0.5}\text{Fe}_{2-x}\text{Cr}_x\text{O}_4$ ($0 \leq x \leq 0.5$) 铁氧体, 并研究 Cr 离子掺杂对铁氧体结构、电学及磁学性能的影响。粉末 X 射线衍射结果表明, 所有制备的样品没有杂相, 均生成结晶良好的纯尖晶石结构。随着 Cr 离子掺杂量增加, 样品的晶格常数和微晶尺寸逐渐减少。磁性测量结果表明, 饱和磁化强度随 Cr 离子掺杂而大幅度减少, 从未掺杂时的 $73.5 \text{ A} \cdot \text{m}^2/\text{kg}$ 减少到掺杂比分为 0.5 时的 $46.3 \text{ A} \cdot \text{m}^2/\text{kg}$ 。室温电阻率随着 Cr 离子的掺杂增加至少 4 个数量级, 在掺杂比分为 0.5 的样品中达到 $1.1 \times 10^8 \Omega \cdot \text{cm}$ 。所有尖晶石样品的介电常数随着频率的增加单调减小, 表现出正常的介电色散行为。介电常数随 Cr 离子掺杂量的变化趋势与电阻率随 Cr 离子掺杂量的变化趋势相反, 掺杂导致 $\text{Fe}^{2+}/\text{Fe}^{3+}$ 电偶极子数量减少, 表明铁氧体中极化机制和导电机制存在着内在的关联。

关键词: NiZn 铁氧体; Cr 离子掺杂; 电阻率; 介电性能; 饱和磁化强度

(Edited by Xiang-qun LI)